AMERICAN SOCIETY FOR MICROBIOLOGY | Applied and Environmental Microbiology®

GENETICS AND MOLECULAR BIOLOGY

The Phospholipid:Diacylglycerol Acyltransferase-Mediated Acyl-Coenzyme A-Independent Pathway Efficiently Diverts Fatty Acid Flux from Phospholipid into Triacylglycerol in *Escherichia coli*

Lian Wang,[a] Shan Jiang,[a] Wen-Chao Chen,[a,b,c,d] Xue-Rong Zhou,[e] Ting-Xuan Huang,[a] Feng-Hong Huang,[a,b,c,d] Xia Wan[a,b,c,d]

[a]Oil Crops Research Institute of the Chinese Academy of Agricultural Sciences, Wuhan, People's Republic of China
[b]Key Laboratory of Biology and Genetic Improvement of Oil Crops, Ministry of Agriculture, Wuhan, People's Republic of China
[c]Oil Crops and Lipids Process Technology National & Local Joint Engineering Laboratory, Wuhan, People's Republic of China
[d]Hubei Key Laboratory of Lipid Chemistry and Nutrition, Wuhan, People's Republic of China
[e]CSIRO Agriculture and Food, Canberra, Australian Capital Territory, Australia

Lian Wang, Shan Jiang, and Wen-Chao Chen are co-first authors. The order of names was determined by increasing seniority.

ABSTRACT Researchers have long endeavored to accumulate triacylglycerols (TAGs) or their derivatives in easily managed microbes. The attempted production of TAGs in *Escherichia coli* has revealed barriers to the broad applications of this technology, including low TAG productivity and slow cell growth. We have demonstrated that an acyl-CoA-independent pathway can divert phospholipid flux into TAG formation in *E. coli* mediated by *Chlamydomonas reinhardtii* phospholipid:diacylglycerol acyltransferase (CrPDAT) without interfering with membrane functions. We then showed the synergistic effect on TAG accumulation via the acyl-CoA-independent pathway mediated by PDAT and the acyl-CoA-dependent pathway mediated by wax ester synthase/acyl-CoA:diacylglycerol acyltransferase (WS/DGAT). Furthermore, CrPDAT led to synchronous TAG accumulation during cell growth, and this could be enhanced by supplementation of arbutin. We also showed that rationally mutated CrPDAT was capable of decreasing TAG lipase activity without impairing PDAT activity. Finally, ScPDAT from *Saccharomyces cerevisiae* exhibited similar activities as CrPDAT in *E. coli*. Our results suggest that the improvement in accumulation of TAGs and their derivatives can be achieved by fine-tuning of phospholipid metabolism in *E. coli*. Understanding the roles of PDAT in the conversion of phospholipids into TAGs during the logarithmic growth phase may enable a novel strategy for the production of microbial oils.

IMPORTANCE Although phospholipid:diacylglycerol acyltransferase (PDAT) activity is presumed to exist in prokaryotic oleaginous bacteria, the corresponding gene has not been identified yet. In this article, we have demonstrated that an acyl-CoA-independent pathway can divert phospholipid flux into TAG formation in *Escherichia coli* mediated by exogenous CrPDAT from *Chlamydomonas reinhardtii* without interfering with membrane functions. In addition, the acyl-CoA-independent pathway and the acyl-CoA-dependent pathway had the synergistic effect on TAG accumulation. Overexpression of *CrPDAT* led to synchronous TAG accumulation during cell growth. In particular, CrPDAT possessed multiple catalytic activities, and the rational mutation of CrPDAT led to the decrease of TAG lipase activity without impairing acyltransferase activity. The present findings suggested that applying PDAT in *E. coli* or other prokaryotic microbes may be a promising strategy for accumulation of TAGs and their derivatives.

Citation Wang L, Jiang S, Chen W-C, Zhou X-R, Huang T-X, Huang F-H, Wan X. 2020. The phospholipid:diacylglycerol acyltransferase-mediated acyl-coenzyme A-independent pathway efficiently diverts fatty acid flux from phospholipid into triacylglycerol in *Escherichia coli*. Appl Environ Microbiol 86:e00999-20. https://doi.org/10.1128/AEM.00999-20.

Editor Rebecca E. Parales, University of California, Davis

Address correspondence to Xia Wan, wanxia@oilcrops.cn.

Received 29 April 2020
Accepted 6 July 2020
Accepted manuscript posted online 17 July 2020
Published 1 September 2020

KEYWORDS phospholipid:diacylglycerol acyltransferase, protein engineering, triacylglycerol, wax ester synthase/acyl-CoA:diacylglycerol acyltransferase

The global demand for oils and oil-based products has been increasing constantly over recent decades. Renewable microbial oils, such as microbial triacylglycerol (TAG), are expected to play a crucial role in providing a sustainable source for oils and their derivatives. TAGs are the important energy storage lipids with highly reduced carbon molecules found in eukaryotes and a few oleaginous bacteria. TAGs can be synthesized via multiple pathways (1–4). TAG synthesis via the acyl-CoA-dependent Kennedy pathway is sequentially catalyzed by glycerol-3-phosphate acyltransferase (GPAT, EC 2.3.1.15), lysophosphatidic acid acyltransferase (LPAAT, EC 2.3.1.51), phosphatidic acid phosphatase (PAP, EC 3.1.3.4), and diacylglycerol acyltransferase (DGAT, EC 3.12.1.20) (5). Nearly 20 years ago, the acyl-CoA-independent pathway mediated by the enzyme phospholipid:diacylglycerol acyltransferase (PDAT, EC 2.3.1.158) was characterized in yeast (*Saccharomyces cerevisiae*) and plants (6). PDAT catalyzes the formation of TAG by transferring an acyl group from the *sn*-2 position of phospholipid (PL) to the *sn*-3 position of diacylglycerol (DAG). Evolutionary analysis reveals that PDATs are present in all examined green plants, including algae, mosses, and lycophytes, as well as fungi (7). Although PDAT activity is presumed to exist in prokaryotic oleaginous bacteria, the corresponding gene has not been identified yet (8, 9).

PDATs participate in regulation of membrane lipid turnover, degradation, and TAG synthesis (10–12). Previous investigations indicate that DGAT and PDAT play overlapping roles in TAG synthesis. In yeast and the unicellular green microalga *Chlamydomonas reinhardtii*, PDATs contribute to TAG production under favorable growth conditions or during the log phase, while DGATs seem to be more essential for TAG synthesis during the stationary phase (10, 13). AtPDAT1 from *Arabidopsis thaliana* has a much higher impact than AtDGAT1 on TAG synthesis in leaves, whereas AtDGAT1 is a major contributor to TAG synthesis in developing seeds (14). In addition, neither AtPDAT1 overexpression nor the knockout change lipid content or fatty acid composition of seed oils, suggesting that AtDGAT1 compensates for the function of AtPDAT1 (15).

Despite the fact that the physiological functions of PDAT seem conserved among yeasts, algae, and plants, its biochemical characteristics vary in some aspects. Of all the discovered PDATs, the biochemical characteristics of CrPDAT from *C. reinhardtii* have been investigated in the most detail (10). CrPDAT exhibits less activity with phosphatidylethanolamine (PE) compared to phosphatidylcholine (PC). Specifically, CrPDAT has a preference for anionic PL, including phosphatidic acid (PA), phosphatidylserine (PS), phosphatidylinositol (PI), and phosphatidylglycerol (PG), over the cationic PC and PE (10). In contrast, AtPDAT and ScPDAT from *Saccharomyces cerevisiae* show preference for PE over PC as the acyl donor *in vitro* (13, 15). In addition to typical PDAT activity, CrPDAT also possesses lipase activity toward both TAGs and various PLs, whereas ScPDAT shows phospholipase activity (10, 13). However, no lipase activity has been described for AtPDAT (15). Although the motif (G/A/S-X-S-X-G) conserved among the α/β hydrolase family is also essential for the lipase activity (15), the catalytic site for lipase activity has not been confirmed for any PDAT (16). Precise information about the lipase active or binding sites is limited mainly due to the lack of structure information of any membrane-bound PDATs.

Escherichia coli is an ideal bacterial cell factory because it is a highly studied model system with well-developed genetic systems that is also easy to culture in the laboratory. *E. coli* has been employed to produce high levels of fatty acids and their derivatives (17). *E. coli* does not produce any TAGs naturally (18), mainly due to the lack of wax ester synthase/acyl-CoA:diacylglycerol acyltransferase (WS/DGAT), which catalyzes the last and rate-limiting step of the acyl-CoA-dependent TAG synthesis pathway (19). The WS/DGAT-mediated acyl-CoA-dependent pathway has been successfully introduced into *E. coli* for the production of regular TAGs or TAGs rich in medium-chain fatty acids (20, 21). Early strategies attempting the accumulation of TAGs were focused

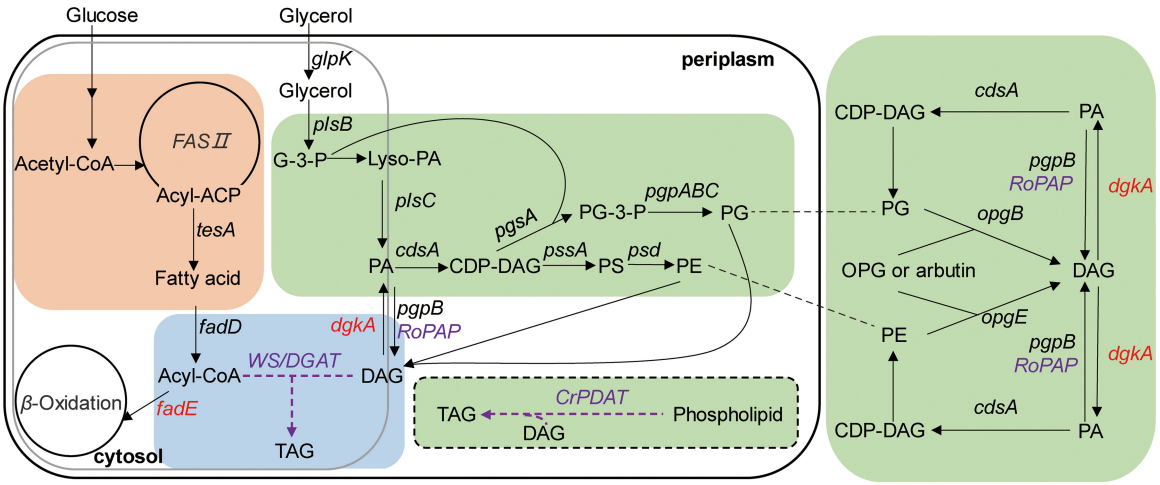

FIG 1 Engineering of *E. coli* cells for TAG accumulation. Heterologous genes are highlighted in purple. Deleted genes are shown in red. G-3-P, glycerol-3-phosphate; Lyso-PA, lysophosphatidic acid; PA, phosphatidic acid; DAG, diacylglycerol; TAG, triacylglycerol; CDP-DAG, cytidine-diphosphate-diacylglycerol; PG-3-P, phosphatidylglycerol-3-phosphate; PG, phosphatidylglycerol; PS, phosphatidylserine; PE, phosphatidylethanolamine; *WS/DGAT*, wax ester synthase/acyl-CoA:diacylglycerol acyltransferase gene; *RoPAP*, phosphatidic acid phosphatase gene from *R. opacus* PD630; *CrPDAT*, phospholipid:diacylglycerol acyltransferase gene from *C. reinhardtii*; *tesA*, acyl-CoA thioesterase I gene; *fadD*, fatty acyl-CoA synthetase gene; *fadE*, acyl-CoA dehydrogenase gene; *glpK*, glycerol kinase gene; *plsB*, glycerol-3-phosphate acyltransferase gene; *plsC*, 1-acylglycerol-3-phosphate O-acyltransferase gene; *dgkA*, diacylglycerol kinase gene; *pgpB*, phosphatidylglycerophosphatase B gene; *cdsA*, CTP:2,3,4-saturated L-phosphatidate cytidylyltransferase gene; *pgsA*, phosphatidylglycerophosphate synthase gene; *pgpABC*, phosphatidylglycerophosphatase ABC gene; *pssA*, phosphatidylserine synthase gene; *psd*, phosphatidylserine decarboxylase gene; *opgE*, phosphoethanolamine transferase gene; *opgB*, phosphoglycerol transferase I gene; OPG, osmoregulated periplasmic glucans.

on the enhancement of fatty acid and/or acyl-CoA synthesis or on blocking the degradation of fatty acid and/or TAGs (20, 22–24).

Membrane PLs and storage TAGs compete for acyl flux; thus, we hypothesized that TAG accumulation might be achieved by diverting fatty acids from PLs to TAGs in *E. coli*. *E. coli* cells have the ability to accumulate abundant PEs (about 75% of total PLs) and PGs (20% of total PLs) (25), which are available substrates for TAG formation catalyzed by CrPDAT. In addition, DAGs, which are by-products generated by the osmo-regulated periplasmic glucan (OPG) biosynthesis pathway, are strictly regulated (26), but they can be greatly enhanced by overexpression of the phosphatidylglycerol phosphatase gene *pgpB* or deletion of the diacylglycerol kinase gene *dgkA* (18, 27). Alternatively, DAG availability may be enhanced by supplementing with arbutin via tuning of the membrane-derived oligosaccharide (MDO) biosynthesis pathway (18). Arbutin is a hydroquinone glucoside compound existing mainly in plants, including bearberry, wheat, and pear (28). In *E. coli*, arbutin can be used as an artificial β-glucoside acceptor for glycerolphosphate, which is transferred from PG and mediated by OpgB (29), or from PE mediated by OpgE (26) (Fig. 1). Previous results revealed that *dgkA*-knockout *E. coli* cells were unable to grow on medium containing arbutin due to the lethal accumulation of DAGs (30), suggesting that DAG levels are probably stimulated by the supplementation of arbutin.

In this report, we first reconstructed the CrPDAT-mediated acyl-CoA-independent TAG synthesis pathway in *E. coli*, even though such a pathway has not been identified in any prokaryotic microbes (Fig. 1). We then demonstrated the synergistic effects of CrPDAT and the WS/DGAT of *Acinetobacter baylyi* ADP1 (AtfA) on TAG accumulation. Furthermore, CrPDAT led to synchronous TAG accumulation during cell growth with enhancement following the supplementation of arbutin. Finally, we showed that rationally mutated CrPDAT possessed the ability to decrease TAG lipase activity without impairing PDAT activity.

RESULTS AND DISCUSSION

Overexpression of a solo *CrPDAT* in an *E. coli* double mutant led to TAG accumulation. To the best of our knowledge, no PDAT-encoding gene has been

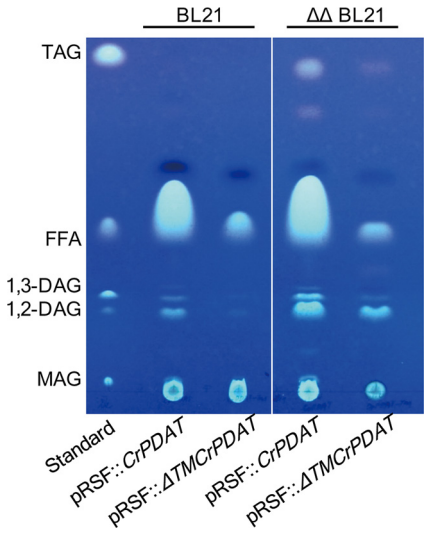

FIG 2 Overexpression of a solo *CrPDAT* or Δ*TMCrPDAT* in *E. coli* BL21 and ΔΔBL21. Cells were cultured in auto-induction medium supplemented with 3% glycerol with shaking at 200 rpm at 37°C for 48 h. TLC was carried out on lipids extracted from 20 mg of dried recombinant cells. ΔΔBL21, knockout of *dgkA* and *fadE* in *E. coli* BL21(DE3); CrPDAT, PDAT from *C. reinhardtii*; ΔTMCrPDAT, CrPDAT without a transmembrane domain.

identified from any prokaryotic oleaginous microorganism to date. Thus, we were interested in testing whether heterologous PDAT could convert PLs into TAGs in *E. coli*. An earlier report showed that the truncated ΔTMCrPDAT (CrPDAT without a transmembrane domain) had higher PDAT activity than a full-length CrPDAT *in vitro* enzyme test (10). Unfortunately, overexpression of a solo *CrPDAT* or Δ*TMCrPDAT* did not result in any detectable TAG accumulation in *E. coli* BL21(DE3) (Fig. 2). We next sought to delete the acyl-CoA dehydrogenase encoded by the gene *fadE* and the diacylglycerol kinase encoded by the gene *dgkA* to generate a double mutant strain designated ΔΔBL21 to elevate the DAG level and prevent the degradation of acyl-CoA (see Fig. S1 in the supplemental material). The results of thin-layer chromatography (TLC) showed that overexpressing *CrPDAT* in ΔΔBL21 led to obvious TAG accumulation (Fig. 2). Compared to wild-type *E. coli*, the DAG levels in ΔΔBL21 cells were greatly enhanced, especially 1,2-DAG. This suggested that the double deletion was beneficial for circumventing the DAG bottleneck and thus promoting TAG synthesis. More importantly, we demonstrated that TAGs could be produced from PL pools via the acyl-CoA-independent pathway by CrPDAT in this *E. coli* double mutant. Transmission electron microscopy observation showed no obvious difference in cell shape between the control and the engineered cells harboring *CrPDAT* during their growth, suggesting that overexpressing *CrPDAT* did not interfere with membrane functions (Fig. S2). In addition, no abnormal phenotype was observed during the growth (data not shown).

Only full-length CrPDAT resulted in obvious TAG synthesis in *E. coli* (Fig. 2). In contrast, previous *in vitro* results revealed that the truncated ΔTMCrPDAT exhibited much higher activities than full-length CrPDAT (10). In addition, an N-terminal deletion version of ScPDAT was highly active *in vitro*, suggesting that the membrane-spanning region was not essential for ScPDAT activity as well (13). The results presented here could be explained by the differences between *in vivo* and *in vitro* conditions. We predicted that the truncated CrPDAT might result in inappropriate folding or instability in *E. coli*. Western blot analysis with anti-His-tag antibody showed that ΔTMCrPDAT exhibited a lower steady-state level of protein than that of full-length CrPDAT (Fig. S3), suggesting the potential instability of the truncated form.

Synergistic effect on TAG production by coexpressing WS/DGAT and CrPDAT. PDAT and DGAT play overlapping roles in TAG synthesis in algae and plants (10, 14). In addition, we previously constructed TAG-producing *E. coli* by overexpressing the

bacterial WS/DGAT- and PAP-encoding genes *atfA* (from *Acinetobacter baylyi*) and *RoPAP* (from *Rhodococcus opacus*) (21). Therefore, we investigated if expressing CrPDAT would further increase TAG levels. The results indicated that coexpressing *atfA* and *RoPAP* along with *CrPDAT* in ΔΔBL21 indeed enhanced the cellular TAG levels further, from 0.1% TAG (wt/wt cell dry weight [CDW]) in the cells without CrPDAT to 2.3% TAG (corresponding to 64.4 mg/liter) (Fig. 3a and 4a). Of interest, a strong synergistic effect was observed in the strain ΔΔPA (ΔΔBL21 harboring *atfA*, *RoPAP*, and *CrPDAT*), as only less than 0.1% TAG was produced by expressing either a solo *CrPDAT* or the combination of *atfA* and *RoPAP* in ΔΔBL21 (Fig. 3a).

Moreover, overexpression of a solo *CrPDAT* in ΔΔBL21 led to a 1.8-fold increase in biomass (6.8 g/liter) compared to that in ΔΔBL21 harboring empty vector (3.7 g/liter). In contrast, individual overexpression of *atfA* or *RoPAP* did not obviously affect the biomass (3.8 g/liter). A similar observation was obtained in *Arabidopsis*, but the mechanism was not characterized (31). We also noticed that the cellular total fatty acid levels were greatly upregulated in ΔΔBL21 harboring *CrPDAT*, leading to a 2.3-fold increase compared to the control strain (208.9 versus 92.8 mg/liter). In addition, CrPDAT did not alter the fatty acid profile (data not shown). Accumulation of large amounts of TAGs with a concomitant increase in total fatty acids (TFAs) suggested an increase in the rate of fatty acid synthesis. This result was in accordance with the phenomenon of *AtPDAT1* overexpression (14). Compared to the combination of *atfA* and *RoPAP*, CrPDAT alone also caused drastic increases in free fatty acids (FFAs) and DAGs (Fig. 3a). Such increases were probably caused by the TAG lipase activity of CrPDAT (10).

Our previous study and reports by other labs demonstrated that a thermophilic tDGAT (DGAT from *Thermomonospora curvata*) was more efficient than AtfA for TAG synthesis in the engineered *E. coli* (21, 32). However, the combined expression of *tDGAT* and *RoPAP* along with *CrPDAT* (designated strain ΔΔPT) yielded 16.3 mg/liter of TAGs, which was only one-third of the levels in ΔΔPA (Fig. 3a). We also observed that ΔΔPT led to the TAGs being dominated by C_{10}-C_{14} fatty acids (47.2% of total), whereas the proportion of long-chain fatty acids, including $C_{16:0}$, $C_{16:1}$, and $C_{18:1}$, had significantly dropped (Fig. 3b). The fatty acid composition in cellular FFA was changed as well, with increases in the proportions of both $C_{14:0}$ and the monounsaturated fatty acids $C_{16:1}$ and $C_{18:1}$ (Fig. 3c). We previously observed that tDGAT also had the ability to facilitate incorporation of large amounts of C_{14} fatty acids into glycerol backbones (21). Therefore, tDGAT might exhibit a preference for tailored acyl-CoAs in *E. coli*. The reduced proportion of TAG in the strain ΔΔPT might be caused by differential substrate selectivity of tDGAT.

To alleviate the metabolic burden, all three candidate genes, *CrPDAT*, *atfA*, and *RoPAP*, were then rearranged into pRSFDuet-1 or pCDFDuet-1 (Table 1) to generate the strains ΔΔRSF-PA or ΔΔCDF-PA. However, assembly of the three genes into one vector (pRSFDuet-1 or pCDFDuet-1) did not lead to higher TAG production than the strain ΔΔPA harboring two separate vectors (Fig. S4A). Although the biomass of ΔΔRSF-PA was higher than that of the other strains, its corresponding TAGs dropped substantially (Fig. S4B). Therefore, the ΔΔPA strain was used in the following tests.

Shortening the incubation time and supplementation of the medium with arbutin-enhanced TAG synthesis in the engineered *E. coli*. Considering that the contribution of CrPDAT to TAG synthesis is mainly during the logarithmic growth phase in *C. reinhardtii*, and that CrPDAT also plays a role in TAG degradation, as it possesses TAG lipase activity (10), the time course for TAG production in the strain ΔΔPA was then investigated. The results showed that the TAG yield from the strain ΔΔPA reached 66.6 mg/liter by 24 h, and extension of the incubation time to 36 or 48 h did not further increase the TAG yield (Fig. 4a). This observation demonstrated that the combinational expression of CrPDAT and AtfA led to higher TAG productivity due to the synchronous TAG accumulation with cell growth.

Arbutin as an artificial β-glucoside acceptor that participates in turnover of PG and PE, and supplementation of arbutin into the medium is reported to redirect PG and PE into DAG (26). Thus, we speculated that TAG synthesis might be enhanced by supple-

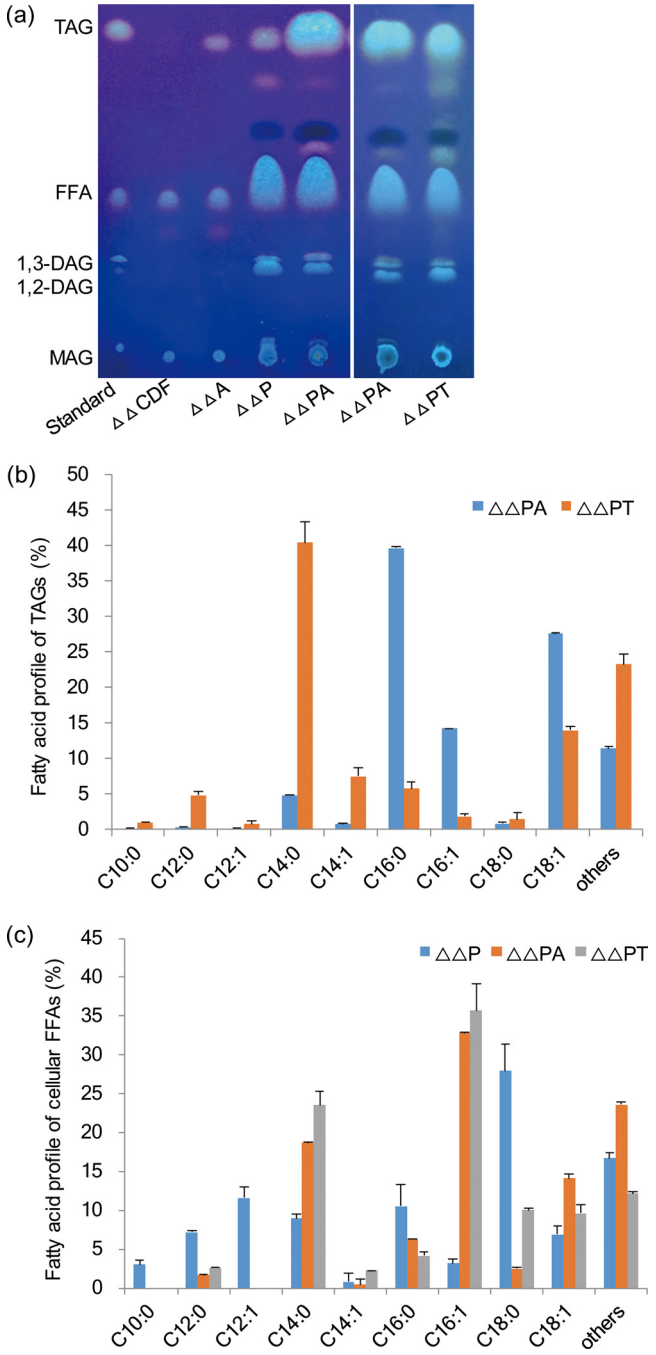

FIG 3 Synergistic effects of CrPDAT and WS/DGAT on TAG content and fatty acid profile. (a) Thin-layer chromatography (TLC) result of neutral lipid profile. (b) Fatty acid profiles of cellular TAGs extracted from ΔΔPA and ΔΔPT. (c) Fatty acid profiles of cellular FFAs extracted from ΔΔP, ΔΔPA, and ΔΔPT. Cells were cultured in auto-induction medium with 3% glycerol at 37°C with shaking at 200 rpm for 48 h. Lipids were extracted from 20 mg of dried recombinant cells. ΔΔCDF, ΔΔBL21 harboring pCDFDuet-1; ΔΔA, ΔΔBL21 harboring pCDFDuet::*atfA*::*RoPAP*; ΔΔP, ΔΔBL21 harboring *CrPDAT*; ΔΔPA, ΔΔBL21 harboring *CrPDAT*, *atfA*, and *RoPAP*; ΔΔPT, ΔΔBL21 harboring *CrPDAT*, *tDGAT*, and *RoPAP*. All data are the mean ± standard deviation (shown as error bar) from triplicate samples.

mentation of arbutin. The effects of arbutin at different concentrations on TAG accumulation in the ΔΔPA strain were investigated. Results showed that the supplementation of medium with 4.6 g/liter arbutin led to a 61.7% increase in TAG yield, reaching up to 108.3 mg/liter of TAGs after the cells were incubated for 5 h (Fig. 4b). Although the supplementation of a higher concentration of arbutin (9.3 g/liter) resulted in the

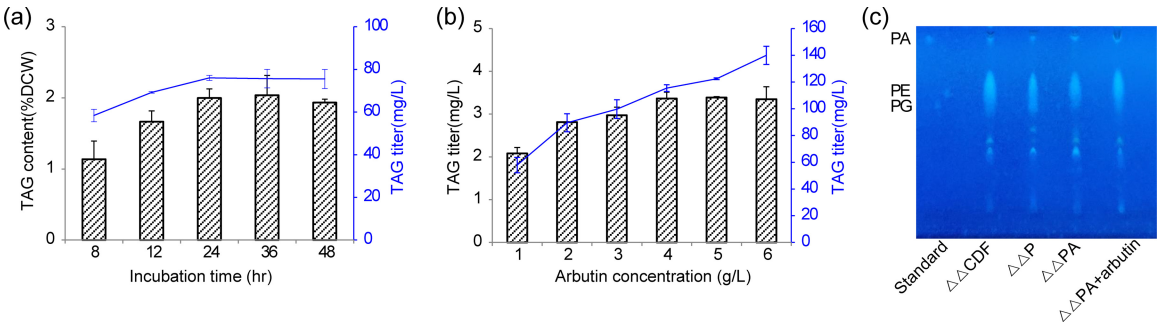

FIG 4 Effects of incubation time (a) and arbutin concentration (b) on TAG content and TAG titer of the ΔΔPA strain and the TLC showing the phospholipid profile compared to its parental strains (c). Cells were cultured in auto-induction medium with 3% glycerol at 37°C with shaking at 200 rpm. All data are the mean ± standard deviation (shown as error bar) from triplicate samples.

highest percentage of TAG, the cell biomass was drastically decreased. Indeed, the TAG yield was not further enhanced with increased arbutin concentrations (Fig. 4b). Meanwhile, the PL content and profiles from the ΔΔPA strain did not change when incubated with 4.6 g/liter of arbutin (Fig. 4c). In addition, the fatty acid profile of the TAG fraction was not obviously affected by the supplementation of arbutin. These results suggested that in addition to pushing PAs toward DAG synthesis and downregulation of DAG turnover, redirection of osmo-regulated periplasmic glucan (OPG) synthesis into DAGs was an alternative way for enhancement of TAG accumulation. However, supplementation of arbutin into the medium to enhance the TAG production is not economically feasible. Recently, the arbutin biosynthetic pathway has been reconstructed in *E. coli* (28). Additional expression of *MNX1* and *AS*, which are two essential genes involved in arbutin biosynthesis might enhance TAG production by the *de novo*-produced arbutin.

Rational mutagenesis of CrPDAT for decreasing TAG lipase activity without impairing acyl transferase activity. We noticed that expression of *CrPDAT* alone or a combined expression of *CrPDAT* and *atfA* in ΔΔBL21 greatly elevated the cellular FFA levels. In contrast to *CrPDAT*, individual expression of *atfA* did not lead to an obvious increase in FFA (Fig. 2). CrPDAT has been demonstrated to be a multifunctional enzyme possessing TAG lipase activity, which probably causes the TAG degradation, in turn, and an increase in FFAs, especially when *CrPDAT* has been overexpressed (10). Therefore, we carried out the rational mutagenesis of CrPDAT to specifically inhibit the TAG lipase activity.

A three-dimensional (3D) model of CrPDAT (Fig. 5a) was generated using Phyre2 according to the crystal structure of lysosomal phospholipase A2 in complex with isopropyl dodec-11-enylfluorophosphonate (IDFP; PDB: 4X91) as the template. The triolein compound was docked into the binding site of CrPDAT, and the theoretical binding mode of the triolein in the CrPDAT binding site is illustrated in Fig. 5b. Triolein adopted a compact conformation to bind inside the CrPDAT pocket (Fig. 5b). Two of the aliphatic chains of triolein were positioned at the hydrophobic pocket, one surrounded by the residues Val-263, Trp-285, Leu-288, Val-291, Phe-332, Ile-333, and Val-338 and the other surrounded by the residues Phe-262, Val-263, Ala-465, Trp-498, and Met-507, forming a strong hydrophobic binding domain (Fig. 5b). The 3D docking model further suggested that three hydrogen bonds could be formed between the triolein and the residues Phe-262, Ser-401, and His-994, with bond lengths of 2.5, 2.9, and 2.6 Å, respectively. Importantly, the carbonyl "O" of the triolein formed two hydrogen bonds with the residues Lys-461 and Thr-942, with bond lengths of 2.1 and 2.9 Å, respectively. All these interactions probably help triolein to anchor in CrPDAT.

The compounds di-palmitoyl-3-*sn*-phosphatidylethanolamine (PEF) and 1,2-di-palmitoyl-phosphatidyl-glycerole (LHG) were then docked into CrPDAT in the 3D model (Fig. 5b). One of the aliphatic chains of PEF was positioned at hydrophobic pocket 1, surrounded by the residues Val-263, Trp-285, Leu-288, Val-291, Phe-332, Ile-333, Val-338, and Ile-995, while the other PEF aliphatic chain was located at hydrophobic pocket

TABLE 1 Plasmids and strains used in this study

Plasmid or strain	Description	Source or reference
Plasmids		
pCDFDuet-1	Spe^r *ori* CDF *lacI* T7	Novagen
pRSFDuet-1	Kan^r *ori* RSF *lacI* T7	Novagen
pRSF::*CrPDAT*	pRSFDuet-1 containing *CrPDAT*	This study
pRSF::*RcPDAT*	pRSFDuet-1 containing *RcPDAT*	
pRSF::*ScPDAT*	pRSFDuet-1 containing *ScPDAT*	
pRSF::Δ*TMCrPDAT*	pCDFDuet-1 containing *CrPDAT* without a transmembrane domain	This study
pCas9	*repA101*(Ts) *kan* pCas-CAS9 ParaB-Red *lacI*^{q} Ptrc-sgRNA-pMB	37
pTargetF	pMB1::*aadA*::sgRNA	37
pTargetF::*fadE*-sgRNA	pMB1::*aadA*::*fadE*-sgRNA	This study
pTargetF::*dgkA*-sgRNA	pMB1::*aadA*::*dgkA*-sgRNA	This study
pTargetT::*fadE*	pMB1::*aadA*::*fadE*-sgRNA containing deletion cassette of *fadE*	This study
pTargetT::*dgkA*	pMB1::*aadA*::*dgkA*-sgRNA containing deletion cassette of *dgkA*	This study
pCDF::*atfA*::*RoPAP*	pCDFDuet-1 containing *atfA* and *RoPAP*	21
pRSF::*CrPDAT*::*atfA*-RoPAP	pRSFDuet-1 containing *CrPDAT* and *atfA*-RBS-*RoPAP*	This study
pCDF::*atfA-RoPAP*::*CrPDAT*	pCDFDuet-1 containing *atfA*-RBS-*RoPAP* and *CrPDAT*	This study
pRSF::*CrPDAT*-Phe-262-Gly	pRSFDuet-1 containing *CrPDAT*-Phe-262-Gly	This study
pRSF::*CrPDAT*-Phe-262-Ala	pRSFDuet-1 containing *CrPDAT*-Phe-262-Ala	This study
pRSF::*CrPDAT*-Ser-401-Asn	pRSFDuet-1 containing *CrPDAT*-Ser-401-Asn	This study
pRSF::*CrPDAT*-Lys-461-Arg	pRSFDuet-1 containing *CrPDAT*-Lys-461-Arg	This study
pRSF::*CrPDAT*-Lys-461-Thr	pRSFDuet-1 containing *CrPDAT*-Lys-461-Thr	This study
pRSF::*CrPDAT*-Gly-941-Ile	pRSFDuet-1 containing *CrPDAT*-Gly-941-Ile	This study
pRSF::*CrPDAT*-Thr-942-Lys	pRSFDuet-1 containing *CrPDAT*-Thr-942-Lys	This study
pRSF::*CrPDAT*-His-994-Asp	pRSFDuet-1 containing *CrPDAT*-His-994-Asp	This study
E. coli strains		
DH5α	F$^-$ ϕ80d*lacZ*ΔM15 Δ(*lacZYA-argF*)*U169 deoR recA1 endA1 hsdR17*(r_K^- m_K^-) *phoA supE44* λ *thi-1 gyrA96 relA*	TaKaRa Bio
BL21(DE3)	F$^-$ *ompT gal dcm lon hsdS*$_B$(r_B^- m_B^-) λ (DE3)	TaKaRa Bio
BL21Δ*fadE*	Knockout of *fadE* in *E. coli* BL21(DE3)	This study
BL21/pRSF::*CrPDAT*	*E. coli* BL21(DE3) harboring pRSF::*CrPDAT*	This study
BL21/pRSF::Δ*TMCrPDAT*	*E. coli* BL21(DE3) harboring pRSF::Δ*TMCrPDAT*	This study
ΔΔBL21	Knockout of *dgkA* and *fadE* in *E. coli* BL21(DE3)	This study
ΔΔRSF	ΔΔBL21 harboring pRSFDuet-1	This study
ΔΔCDF	ΔΔBL21 harboring pCDFDuet-1	This study
ΔΔP	ΔΔBL21 harboring pRSF::*CrPDAT*	This study
ΔΔBL21/pRSF::Δ*TMCrPDAT*	ΔΔBL21 harboring pRSF::Δ*TMCrPDAT*	This study
ΔΔA	ΔΔBL21 harboring pCDFDuet::*atfA*::*RoPAP*	This study
ΔΔPA	ΔΔBL21 harboring pRSF::*CrPDAT* and pCDFDuet::*atfA*::*RoPAP*	This study
ΔΔPT	ΔΔBL21 harboring pRSF::*CrPDAT* and pCDFDuet::*tDGAT*::*RoPAP*	This study
ΔΔRSF-PA	ΔΔBL21 harboring pRSF::*CrPDAT*::*atfA-RoPAP*	This study
ΔΔCDF-PA	ΔΔBL21 harboring pCDF::*atfA-RoPAP*::*CrPDAT*	This study

2, surrounded by the residues Phe-262, Val-459, Ala-465, Trp-498, and Met-507, forming a strong hydrophobic binding domain (Fig. 5b). In the case of LHG, the predicted hydrophobic pocket 1 was surrounded by Val-263, Trp-285, Phe-332, Val-338, and Ile-995, while hydrophobic pocket 2 had the same amino acids as in the CrPDAT:PEF model.

In addition, the residues Lys-461 and Thr-942 might be crucial for formation of the three hydrogen bonds between the phosphate groups of all three candidates (PEF/LHG/triolein). Furthermore, one of the "O" atoms of the PEF formed a hydrogen bond with the residue Ser-401, and the polar hydrogen of the NH_2 group of PEF formed a hydrogen bond with the residue Gly-941 (Fig. 5b). In contrast, Ser-401 and His-994, with bond lengths of 2.8 and 2.4 Å, respectively, participated in hydrogen bond formation with LHG according to the three-dimensional model.

The above-described molecular simulations in the 3D model gave us a rational explanation of the interactions between CrPDAT and PEF/LHG/triolein. Although five putative amino acid residues, Ser-401, Lys-461, Thr-942, His-994, and Phe-262, were predicted to play key roles in the CrPDAT:triolein model, Phe-262 was the only differential amino acid among three models. Phe-262 was not essential for hydrogen bond formation in either the CrPDAT:PEF or CrPDAT:LHG model. Therefore, mutation of

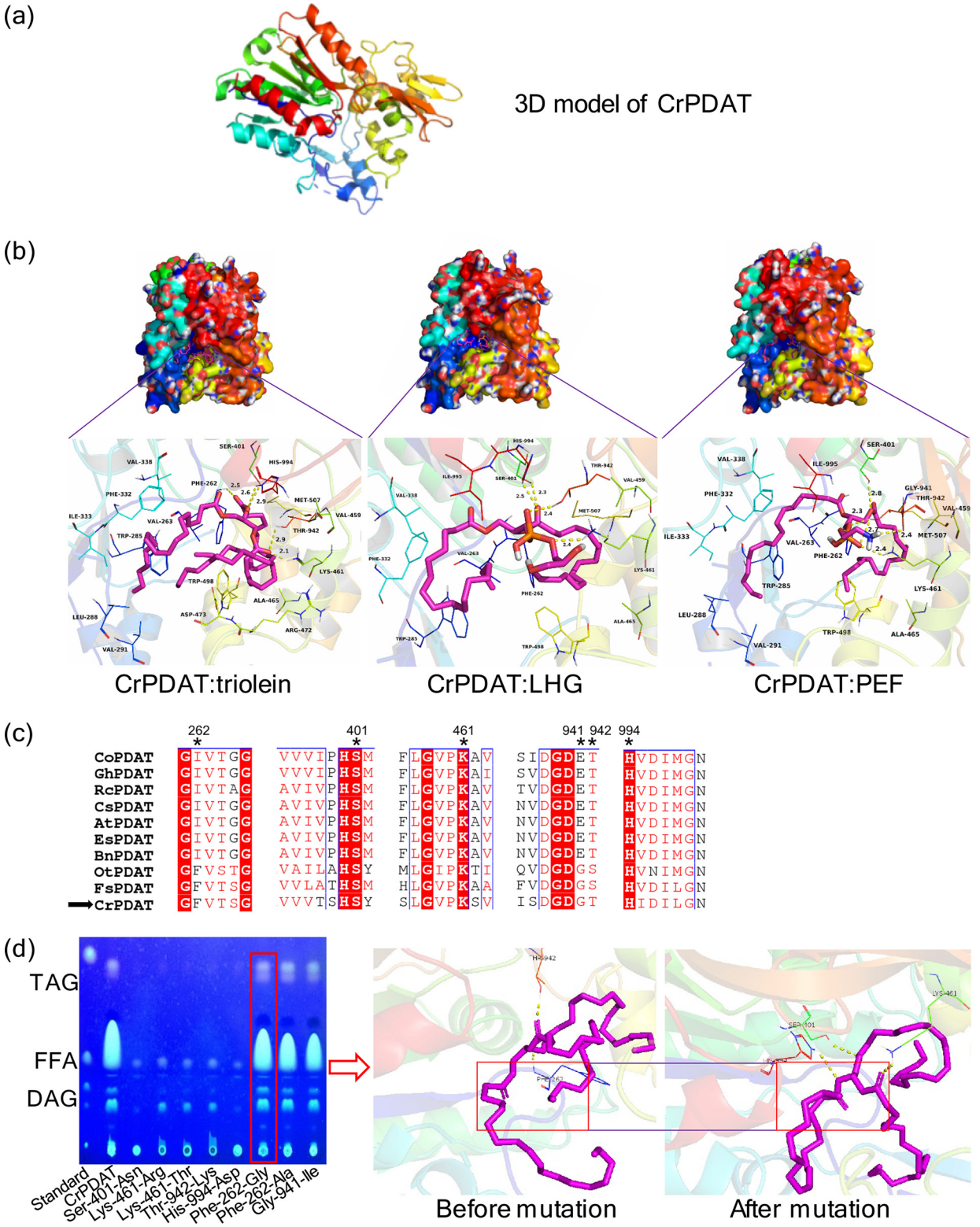

FIG 5 Schematic of the rational mutagenesis system workflow. The aim of this system is to decrease TAG lipase activity without impairing acyltransferase activity of CrPDAT (a). Three docking models of triolein (left), LHG (middle), and PEF (right) to CrPDAT were simulated (b). The essential amino acids involved in hydrogen bond formation were predicted. Sequence alignment of 10 selected PDATs was carried out to identify the distribution of those predicted essential amino acids (c). Identical residues are shown in white on a red background, while similar residues are shown in red. The predicted binding sites are indicated by black asterisks. The ability of the rational designed mutants to accumulate TAG was determined by TLC (d). The binding model of the positive mutant (Phe-262-Gly) was reconstructed by molecular docking to confirm the loss of the hydrogen bond between CrPDAT and triolein (d).

TABLE 2 Analysis of three mutants generated by rational mutagenesis of CrPDAT[a,b]

Strain	Biomass (g/liter)	TAG (μg/mg CDW)	TAG (mg/liter)	FFA (mg/liter)	TFA (mg/liter)
ΔΔP	6.8 ± 0.2	0.9 ± 0.2	6.1 ± 0.8	155.9 ± 15.2	208.9 ± 9.6
Mutant phe-262-Gly	6.3 ± 0.3	1.0 ± 0.1	6.2 ± 0.5	128.6 ± 25.5[c]	241.4 ± 27.3
Mutant Phe-262-Ala	5.1 ± 0.8	0.8 ± 0.1	4.1 ± 0.1	93.9 ± 30.6[c]	131.4 ± 68.1
Mutant Gly-941-Ile	4.9 ± 0.4	0.9 ± 0.1	4.4 ± 0.3	63.1 ± 17.2[c]	158.9 ± 11.4

[a]ΔΔP, ΔΔBL21 harboring pRSF::*CrPDAT*; TAG, triacylglycerol; FFA, free fatty acid; TFA, total fatty acid; CDW, cell dry weight.
[b]Cells were cultivated in ZYP-5052 auto-induction medium with 3% glycerol at 37°C and shaking at 200 rpm for 48 h. All data are the means ± standard deviations from triplicates.
[c]The significance between ΔΔP and each mutant (Student's *t* test; $P < 0.05$).

Phe-262 might alter the hydrogen bond between CrPDAT and triolein. We also noticed that Phe-262 was involved in hydrophobic pocket formation in both the CrPDAT:PEF and CrPDAT:LHG models (Fig. 5b); thus, mutation of Phe-262 might also affect acyl transferase activity.

Moreover, sequence alignment of selected PDAT proteins was carried out. Among the six predicted amino acid residues, four of them, Ser-401, Lys-461, Thr-942, and His-994, were conserved among PDATs, while Phe-262 and Gly-941 were less conservative (Fig. 5c). Notably, Ser-401 and His-994 were also part of the catalytic triad (Ser-Asp-His) (7).

Based on the above-described prediction, we constructed a series of mutants (Table 1). We first investigated the neutral lipid profile of these mutants by using TLC. Five mutants, Ser-401-Asn, Lys-461-Arg, Lys-461-Thr, Thr-942-Lys, and His-994-Asp, were unable to synthesize any detectable TAGs (Fig. 5d), suggesting that these amino acid residues were essential to PDAT activity. Then, we further analyzed the other three mutants which could produce TAGs. Only mutant Phe-262-Gly led to a 17.5% decrease in FFA levels without affecting TAG synthesis (Table 2 and Fig. 5d). An *in vitro* enzyme test also demonstrated that the TAG lipase activity of mutant Phe-262-Gly decreased, leading to more stable TAG and less produced FFA compared with that of CrPDAT (Fig. S5). In contrast, although the FFA levels in the Phe-262-Ala and Gly-941-Ile mutants decreased by 39.7% and 59.5%, TAGs from these two mutants were also reduced by 32.7% and 27.5%, respectively (Table 2 and Fig. 5d). There was also a side effect of the reduced biomass in the mutants Phe-262-Ala and Gly-941-Ile, so these were not the preferable choices for enhancing TAG production. In addition, we found that the Gly-941-Ile mutant exhibited a much lower growth rate than the wild-type *E. coli* and other mutants during the exponential growth phase (0 to 8 h), although the difference became insignificant after reaching the stationary growth phase. Nevertheless, mutant Phe-262-Gly was a beneficial candidate for TAG accumulation. Mutation of Phe-262 to other residues might lead to further reduced lipase activity.

CrPDAT orthologues resulted in TAG accumulation in *E. coli*. We next investigated if other PDATs could play similar roles in diverting fatty acids from PLs into TAGs in strain ΔΔBL21. According to the motif pattern of the PDAT proteins from plants, fungi, and microalgae, the major difference among CrPDAT and other PDATs is the existence of three long linkers (Fig. 6). Cladogram analysis indicated that plant source RcPDAT (PDAT from *Ricinus communis*) and yeast ScPDAT reside in the different groups from CrPDAT (Fig. 6). TLC results indicated that overexpression of *ScPDAT* in ΔΔBL21 led to obvious DAG and TAG accumulation, whereas *RcPDAT* did not (Fig. 7). In addition, either *RcPDAT* or *ScPDAT* overexpression caused an increase in biomass, to the same level of 5.4 g/liter, relative to the 3.7 g/liter of biomass from the ΔΔBL21 strain harboring empty vector (Table 3). This was similar to our above-described observation that biomass was increased to 6.8 g/liter by *CrPDAT* overexpression and again confirmed our previous hypothesis that overexpression of *PDAT* in the engineered *E. coli* could lead to synchronous TAG production with cell growth.

Considering that ScPDAT shows a preference for PE over PC, while CrPDAT prefers anionic PLs (10, 13), we speculated that the combinational expression of *ScPDAT* and *CrPDAT* might further increase TAG levels via full utilization of PLs. However, coexpress-

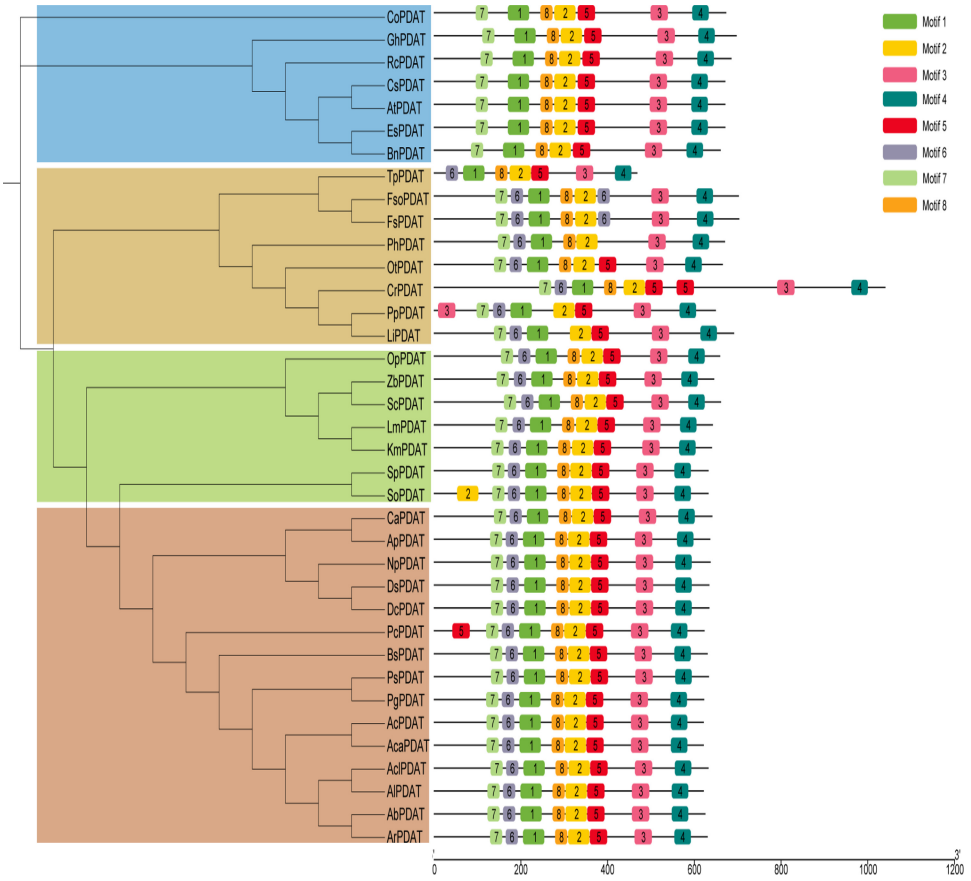

FIG 6 Cladogram (left) and motif patterns (right) of PDAT proteins from representative plants, fungi, and algae. The detailed information on each PDAT protein is listed in Table S2.

ing *CrPDAT* and *ScPDAT* drastically decreased TAG levels to less than 0.01% (Fig. 7), suggesting that the two enzymes did not work coordinately or that PLs were strictly regulated in *E. coli*. In the next step, further downregulation of PL synthesis may be achieved by blocking the expression of the phosphatidylserine decarboxylase gene, *psd*, and/or the phosphatidylserine synthase gene, *pssA*, based on CRISPR interference (CRISPRi) (33) (Fig. 1).

PDATs from castor bean, *Crepis palaestina*, and flax are involved in accumulation of unusual fatty acids, such as ricinoleic acid, vernolic acid, and α-linolenic acid (6, 34, 35). Notably, AtPDAT and ScPDAT also show strong specificity for acyl groups with multiple double bonds or a functional group (13, 15). These findings indicate the that PDATs probably play a vital role in removal of unusual fatty acids from PLs to TAGs. We speculate that these PDATs may be employed to produce TAGs rich in unusual fatty acids via metabolic engineering of microbes.

Conclusions. We demonstrated that a CrPDAT-mediated acyl-CoA-independent pathway could divert fatty acid flux from PLs into TAGs in *E. coli* without impairing membrane functions. Of interest, CrPDAT and AtfA had a synergistic effect on TAG production. Combined expression of CrPDAT and tDGAT altered TAG composition with increased C_{10} to C_{14} fatty acids. Overexpression of *CrPDAT* alone or the *CrPDAT* and *atfA* combination led to synchronous TAG production with cell growth, which resulted in a high level of TAG productivity in 24 h. Supplementation of arbutin into the medium further increased TAG production by altering MDO metabolism. In addition, our experiments with rationally designed CrPDAT mutants revealed that many essential amino acid residues played overlapping roles in both acyltransferase and TAG lipase activity, while only the Phe-262-Gly mutant showed decreased TAG lipase activity without

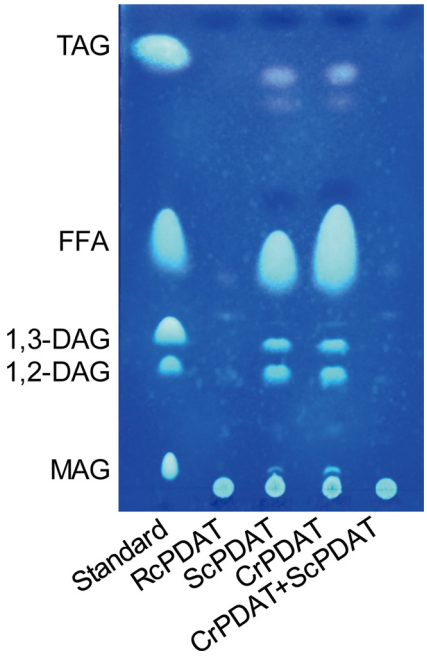

FIG 7 Evaluation of the ability of RcPDAT and ScPDAT for the production of TAG in ΔΔBL21 by using thin-layer chromatography (TLC). RcPDAT, PDAT from *R. communis*; ScPDAT, PDAT from *S. cerevisiae*; CrPDAT, PDAT from *C. reinhardtii*. Cells were cultured in auto-induction medium with 3% glycerol at 37°C with shaking at 200 rpm for 48 h. Lipids were extracted from 20 mg of dried recombinant cells. All data are the mean ± standard deviation from triplicate samples.

interfering acyltransferase activity. Finally, ScPDAT exhibited functions in the engineered *E. coli* similar to CrPDAT. The investigation of the roles of CrPDAT in *E. coli* opens the possibility of utilizing this enzyme for the synthesis of TAGs and other functional lipids in prokaryotic microbes.

MATERIALS AND METHODS

Materials. Chemicals were obtained from Sinopharm Chemical Reagent Co., Ltd. (Shanghai, China) or Sigma-Aldrich Co. (St. Louis, MO, USA). Arbutin was purchased from Adamas Reagent, Ltd. (Shanghai, China). Hexane, chloroform, and methanol were purchased from Merck KGaA (Darmstadt, Germany). T4 DNA ligase and restriction enzymes were purchased from Thermo Fisher Scientific (Beverly, USA). The plasmid miniprep kit, total DNA extraction kit, PCR purification kit, SoSoo cloning kit, and gel extraction kit were purchased from Beijing TsingKe Biotech Co., Ltd. (Beijing, China). *E. coli* DH5α and *E. coli* BL21(DE3) chemically competent cells were purchased from TransGen Biotech (Beijing, China). Standards, including FFA, DAG, monoacylglycerol (MAG), TAG, PA, PE, PG, and GLC-411 were purchased from Nu-Chek (Elysian, MN, USA) or Larodan (Stockholm, Sweden).

Strains, medium, and growth conditions. *E. coli* DH5α was employed for plasmid construction and propagation, while *E. coli* BL21(DE3) was used as the expression strain for TAG accumulation. *E. coli* DH5α cells were cultivated in lysogeny broth (LB; 1% [wt/vol] tryptone, 0.5% [wt/vol] yeast extract, and 1% [wt/vol] NaCl) at 37°C with shaking at 200 rpm. *E. coli* BL21(DE3) cells were cultivated in ZYP-5052 auto-induction medium (36) with 3% glycerol at 37°C and shaking at 200 rpm. Appropriate antibiotics were added at the following concentrations: 50 mg/liter kanamycin or 50 mg/liter spectinomycin.

Plasmid construction. All plasmids used in this study are listed in Table 1. The *CrPDAT* gene from *C. reinhardtii* (GenBank accession number XM_001699696), *ScPDAT* (accession number NP_014405) from

TABLE 3 Evaluation of the ability of three selected PDATs to synthesize TAG[a,b]

Strain/ΔΔBL21 harboring:	Biomass (g/liter)	TAG (μg/mg CDW)	TAG (mg/liter)
pRSF::*CrPDAT*	6.8 ± 0.1	0.9 ± 0.1	6.1 ± 0.1
pRSF::*RcPDAT*	5.4 ± 0.7	0.1 ± 0.0	0.5 ± 0.0
pRSF::*ScPDAT*	5.4 ± 0.1	1.0 ± 0.1	5.4 ± 0.1

[a]CrPDAT, PDAT from *C. reinhardtii*; RcPDAT, PDAT from *R. communis*; ScPDAT, PDAT from *S. cerevisiae*; TAG, triacylglycerol; CDW, cell dry weight.
[b]Cells were cultivated in ZYP-5052 auto-induction medium with 3% glycerol at 37°C and shaking at 200 rpm for 48 h. All data are the means ± standard deviations from triplicates.

TABLE 4 Primers used in this study

Primer	Nucleotide sequence (5′–3′)[a]
CrPDAT-F	CACAGCCAGGATCCGAATTCATGACCACACCGACC
CrPDAT-R	AGCATTATGCGGCCGCAAGCTTTTAGGCTGCCAGCGC
CrPDAT-TMD-F	CACAGCCAGGATCCGAATTCATGGTTGAAGAAGGTCCG
fadE-IF	CCGATTGCCATCACCGTT
fadE-IR	GCGAACTTTGTTGCTACCG
dgkA-IF	CGGTACACTGATATTGACGCTC
dgkA-IR	GCGTCGGCGGCATACCTGT
dgkA-OF	GGGAAATTCTGTGGTATCCGCTC
dgkA-OR	CGGCGGCATACCTGTCTGG
CrPDAT-Phe-262-Gly-LR	TCCAGACCGCTGGTAACACCACCCGGAACAATAACAA
CrPDAT-Phe-262-Gly-RF	TTGTTATTGTTCCGGGTGGTGTTACCAGCGGTCTGGA
CrPDAT-Phe-262-Ala-LR	TCCAGACCGCTGGTAACAGCACCCGGAACAATAACAA
CrPDAT-Phe-262-Ala-RF	TTGTTATTGTTCCGGGTGCTGTTACCAGCGGTCTGGA
CrPDAT-Ser-401-Asn-LR	AAAACATTTTCACCATAATTATGGCTGGTCACAACAA
CrPDAT-Ser-401-Asn-RF	TTGTTGTGACCAGCCATAATTATGGTGAAAATGTTTT
CrPDAT-Lys-461-Arg-LR	AGCAGTGCGCTAACACTTCTCGGAACACCCAGGCTGG
CrPDAT-Lys-461-Arg-RF	CCAGCCTGGGTGTTCCGAGAAGTGTTAGCGCACTGCT
CrPDAT-Lys-461-Thr-LR	AGCAGTGCGCTAACACTTGTCGGAACACCCAGGCTGG
CrPDAT-Lys-461-Thr-RF	CCAGCCTGGGTGTTCCGACAAGTGTTAGCGCACTGCT
CrPDAT-Gly-941-Ila-LR	ACTCAGCAGAGGAACCGTAATATCACCGTCGCTAATAT
CrPDAT-Gly-941-Ila-RF	ATATTAGCGACGGTGATATTACGGTTCCTCTGCTGAG
CrPDAT-Thr-942-Lys-LR	AGACTCAGCAGAGGAACCTTACCATCACCGTCGCTAA
CrPDAT-Thr-942-Lys-RF	TTAGCGACGGTGATGGTAAGGTTCCTCTGCTGAGTCT
CrPDAT-His-994-Asp-LR	ATTACCCAGAATATCAATATCTGCGGCTGCTGCTGGA
CrPDAT-His-994-Asp-RF	TCCAGCAGCAGCCGCAGATATTGATATTCTGGGTAAT

[a]Underlining indicates restriction enzyme sites.

S. cerevisiae, and *RcPDAT* (accession number GU989637) from *Ricinus communis* were codon-optimized and chemically synthesized (Table S1). Full-length *CrPDAT*, *ScPDAT*, *RcPDAT*, and *CrPDAT* without the transmembrane domain (Δ*TMCrPDAT*) were inserted separately into pRSFDuet-1 via the EcoRI/HindIII restriction sites. The plasmid pCDF::*atfA*::*RoPAP* was constructed previously (21). Both the *A. baylyi* WS/DGAT gene (*atfA*) and the *Rhodococcus opacus* PD630 PAP gene (*RoPAP*) were inserted into pRSF::*CrPDAT* via KpnI/XhoI to generate pRSF::*CrPDAT*::*atfA-RoPAP*. Then, the *CrPDAT* gene was inserted into pCDFDuet::*atfA-RoPAP* via KpnI/XhoI to generate pCDF::*atfA-RoPAP*::*CrPDAT*. According to the instructions of the SoSoo cloning kit, site-directed mutagenesis of DNA fragments of *CrPDAT* and linearized pRSFDuet-1 were fused by the mixed recombination enzyme in 2× SoSoo mix. The reaction system was incubated for 15 min at 50°C, and then the mixture was transformed into *E. coli* DH5α. Positive mutants were confirmed by sequencing. Primers are listed in Table 4.

Gene deletion with the CRISPR/Cas9 system. Deletion of both the *fadE* gene encoding acyl-CoA dehydrogenase that catalyzes the first step of β-oxidation and the diacylglycerol kinase gene *dgkA* in *E. coli* BL21(DE3) was conducted according to a modified CRISPR/Cas9 system (37). The two-plasmid system comprising pCas and pTarget was applied to delete *fadE* or *dgkA* from the genome of *E. coli* BL21(DE3). A protospacer-adjacent motif (PAM) was chosen by using online software (https://www.atum.bio/eCommerce/cas9/input). The chosen single guide RNA (sgRNA) was then further analyzed with Cas-OFFinder (http://www.rgenome.net/cas-offinder/) to avoid any potential off-target effects. The second structure of the designed sequence was checked by using mfold (http://unafold.rna.albany.edu/?q=mfold/DNA-Folding-Form). The N_{20} sequences of sgRNA-*fadE* and sgRNA-*dgkA* were designed as follows: 5′-GATGTCTCGATGGCTGTGCT-3′ and 5′-TAAAGATATGGGATCCGCCG-3′.

For the knockout of *fadE* and *dgkA*, the deletion cassettes were fused with 200-bp up- and downstream flanking regions of the target genes. The sgRNA fragments of *dgkA* and *fadE* were chemically synthesized and subcloned into SpeI/XhoI sites of pTargetF to generate pTargetF::*dgkA*-sgRNA and pTargetF::*fadE*-sgRNA. pTargetT::*dgkA* and pTargetT::*fadE* were constructed by inserting the corresponding deletion cassette into the HindIII/XhoI-digested pTargetF::*dgkA*-sgRNA and pTargetF::*fadE*-sgRNA, respectively.

BL21(DE3) electro-competent cells harboring pCas were prepared as described previously (37, 38). Arabinose (10 mM) was added to the medium for λ-Red induction. Then, 200 ng of pTargetT::*fadE* was mixed with 100 μl of electro-competent induced cells. The mixture of plasmid and electro-competent cells was chilled on ice for 10 min. After electroporation, the mixture was transferred to 1.5-ml sterile tubes with 1 ml of LB medium and incubated at 30°C for 1 h. Positive mutants were identified by colony PCR and sequencing. pTargetT::*fadE* was cured by incubation with spectinomycin (50 mg/liter) at 30°C.

In the first round of deletion, BL21Δ*fadE* was obtained. Then, BL21Δ*fadE* harboring pCas was used for the deletion of *dgkA*. After a second round of electroporation, pTargetT::*dgkA* was cured by incubation with spectinomycin (50 mg/liter) at 30°C. Then, pCas9 was cured by incubating it overnight at 37°C. The obtained double mutant BL21Δ*fadE* Δ*dgkA*, designated ΔΔBL21, was confirmed by sequencing.

Bioinformatic analysis. TMHMM Server v.2.0 (http://www.cbs.dtu.dk/services/TMHMM/) was used for transmembrane prediction. Protein sequence alignment was conducted with MAFFT (https://www.ebi.ac.uk/Tools/msa/mafft/) (39). Phylogenetic analysis of PDATs was conducted by using MEGA 6.06

with the neighbor-joining method (N-J) (40). Online iTOL (http://itol.embl.de) software was used to visualize the phylogenetic tree (41). Motif occurrences were predicted using the MEME program (http://meme-suite.org/tools/meme) and visualized with TBtools (42).

The three-dimensional model of the CrPDAT was built with Phyre2 (http://www.sbg.bio.ic.ac.uk/phyre2/html/page.cgi?id=index) (43). AutoDock Vina 1.1.2 was used to search for potential binding sites of LHG, PEF, and triolein within CrPDAT (44). The 2D structures of LHG, PEF, and triolein were drawn with ChemBioDraw Ultra 14.0 and converted to a 3D structure with the ChemBio3D Ultra 14.0 package. The AutoDockTools 1.5.6 package was employed to generate the docking input files (45). The best-scoring pose judged by the Vina docking score was chosen and visualized with PyMOL 1.7.6 software (http://www.pymol.org/).

Lipid analysis. Cells were collected by centrifugation and vacuum-dried overnight. Total lipids were extracted from freeze-dried cells as previously described (21). The extracted lipids were separated by TLC using a solvent system (hexane:diethyl ester:acetic acid = 70:30:1, vol/vol/vol) and visualized by spraying with primuline. For separation of PLs, a solvent system consisting of chloroform/methanol/acetic acid/water (90:15:10:3, vol/vol/vol/vol) was used. The bands corresponding to TAG or FFA were scraped from TLC plates into vials and methylated to generate fatty acid methyl esters (FAMEs) (46). FAMEs were then analyzed by using a 7890A gas chromatograph (GC; Agilent Technologies, USA) equipped with a flame ionization detector (FID) and an HP-FFAP column (30 m by 250 μm inside diameter [i.d.], 0.25 μm thickness). For quantification, either 5 μg of $C_{15:0}$-TAG and 5 μg of $C_{15:0}$-FFA (for low levels of TAG or FFA) or 20 μg of $C_{15:0}$-TAG and 10 μg of $C_{15:0}$-FFA were added to the samples as internal standards before lipid extraction. To quantify cellular TFAs, lipids from 2 mg of cell powder were directly methylated to produce corresponding FAMEs and were analyzed with GC as described above.

Microscopy analysis. For detection of the membrane integrity of engineered cells, cells were fixed with 2.5% glutaraldehyde and 2% paraformaldehyde in 0.1 M phosphate buffer (pH 7.4) under vacuum for at least 24 h. Then, the samples were treated with 50, 70, 80, and 95% ethanol sequentially and processed with a mixed solution of acetone and epoxy resin (1:1 for 1 h, then 1:3 for 3 h). After infiltration with epoxy resin and ultrathin-section treatment, the samples were stained with uranyl acetate and lead citrate. The samples were observed with a HT7700 transmission electron microscope (Hitachi High-Tech).

Data availability. All data generated or analyzed during this study are included in this article and its supplemental files.

SUPPLEMENTAL MATERIAL

Supplemental material is available online only.

SUPPLEMENTAL FILE 1, PDF file, 0.7 MB.

ACKNOWLEDGMENTS

We are grateful to Harley Edwards for providing help with English.

We declare that we have no competing interests.

This work was financially supported by the Chinese Academy of Agricultural Sciences (grant numbers Y2020XK25 and CAAS-ASTIP-2016-OCRI), the Ministry of Science and Technology of the People's Republic of China (grant number 2016YFD0501209), and the "3551" Innovative Talent Project of Optics Valley of China (K159).

L.W., S.J., W.-C.C., and X.-R.Z. conceived the project. L.W., S.J., and T.-X.H. carried out experimental work. L.W., W.-C.C., X.-R.Z., and X.W. analyzed and interpreted the data. X.-R.Z., F.-H.H., and X.W. wrote the paper, with all authors assisting in the process.

REFERENCES

1. Waltermann M, Luftmann H, Baumeister D, Kalscheuer R, Steinbuchel A. 2000. Rhodococcus opacus strain PD630 as a new source of high-value single-cell oil? Isolation and characterization of triacylglycerols and other storage lipids. Microbiology 146:1143–1149. https://doi.org/10.1099/00221287-146-5-1143.
2. Olukoshi ER, Packter NM. 1994. Importance of stored triacylglycerols in Streptomyces: possible carbon source for antibiotics. Microbiology 140:931–943. https://doi.org/10.1099/00221287-140-4-931.
3. Theodoulou FL, Eastmond PJ. 2012. Seed storage oil catabolism: a story of give and take. Curr Opin Plant Biol 15:322–328. https://doi.org/10.1016/j.pbi.2012.03.017.
4. Alvarez HM, Steinbuchel A. 2002. Triacylglycerols in prokaryotic microorganisms. Appl Microbiol Biotechnol 60:367–376. https://doi.org/10.1007/s00253-002-1135-0.
5. Kennedy EP. 1961. Biosynthesis of complex lipids. Fed Proc 20:934–940.
6. Dahlqvist A, Stahl U, Lenman M, Banas A, Lee M, Sandager L, Ronne H, Stymne S. 2000. Phospholipid:diacylglycerol acyltransferase: an enzyme that catalyzes the acyl-CoA-independent formation of triacylglycerol in yeast and plants. Proc Natl Acad Sci U S A 97:6487–6492. https://doi.org/10.1073/pnas.120067297.
7. Pan X, Peng FY, Weselake RJ. 2015. Genome-wide analysis of phospholipid:diacylglycerol acyltransferase (PDAT) genes in plants reveals the eudicot-wide PDAT gene expansion and altered selective pressures acting on the core eudicot PDAT paralogs. Plant Physiol 167:887–904. https://doi.org/10.1104/pp.114.253658.
8. Rottig A, Strittmatter CS, Schauer J, Hiessl S, Poehlein A, Daniel R, Steinbuchel A. 2016. Role of wax ester synthase/acyl coenzyme A:diacylglycerol acyltransferase in oleaginous Streptomyces sp. strain G25. Appl Environ Microbiol 82:5969–5981. https://doi.org/10.1128/AEM.01719-16.
9. Arabolaza A, Rodriguez E, Altabe S, Alvarez H, Gramajo H. 2008. Multiple pathways for triacylglycerol biosynthesis in Streptomyces coelicolor. Appl Environ Microbiol 74:2573–2582. https://doi.org/10.1128/AEM.02638-07.
10. Yoon K, Han D, Li Y, Sommerfeld M, Hu Q. 2012. Phospholipid:diacylglycerol acyltransferase is a multifunctional enzyme involved in membrane lipid turnover and degradation while synthesizing triacylglycerol in the unicel-

lular green microalga Chlamydomonas reinhardtii. Plant Cell 24:3708–3724. https://doi.org/10.1105/tpc.112.100701.
11. Fan J, Yan C, Roston R, Shanklin J, Xu C. 2014. Arabidopsis lipins, PDAT1 acyltransferase, and SDP1 triacylglycerol lipase synergistically direct fatty acids toward beta-oxidation, thereby maintaining membrane lipid homeostasis. Plant Cell 26:4119–4134. https://doi.org/10.1105/tpc.114.130377.
12. Liu XY, Ouyang LL, Zhou ZG. 2016. Phospholipid: diacylglycerol acyltransferase contributes to the conversion of membrane lipids into triacylglycerol in Myrmecia incisa during the nitrogen starvation stress. Sci Rep 6:26610. https://doi.org/10.1038/srep26610.
13. Ghosal A, Banas A, Stahl U, Dahlqvist A, Lindqvist Y, Stymne S. 2007. Saccharomyces cerevisiae phospholipid:diacylglycerol acyl transferase (PDAT) devoid of its membrane anchor region is a soluble and active enzyme retaining its substrate specificities. Biochim Biophys Acta 1771: 1457–1463. https://doi.org/10.1016/j.bbalip.2007.10.007.
14. Fan J, Yan C, Zhang X, Xu C. 2013. Dual role for phospholipid:diacylglycerol acyltransferase: enhancing fatty acid synthesis and diverting fatty acids from membrane lipids to triacylglycerol in Arabidopsis leaves. Plant Cell 25:3506–3518. https://doi.org/10.1105/tpc.113.117358.
15. Stahl U, Carlsson AS, Lenman M, Dahlqvist A, Huang B, Banas W, Banas A, Stymne S. 2004. Cloning and functional characterization of a phospholipid:diacylglycerol acyltransferase from Arabidopsis. Plant Physiol 135:1324–1335. https://doi.org/10.1104/pp.104.044354.
16. Schrag JD, Cygler M. 1997. Lipases and alpha/beta hydrolase fold. Methods Enzymol 284:85–107. https://doi.org/10.1016/s0076-6879(97)84006-2.
17. Wang C, Pfleger BF, Kim SW. 2017. Reassessing Escherichia coli as a cell factory for biofuel production. Curr Opin Biotechnol 45:92–103. https://doi.org/10.1016/j.copbio.2017.02.010.
18. Janßen HJ, Steinbüchel A. 2014. Production of triacylglycerols in Escherichia coli by deletion of the diacylglycerol kinase gene and heterologous overexpression of atfA from Acinetobacter baylyi ADP1. Appl Microbiol Biotechnol 98:1913–1924. https://doi.org/10.1007/s00253-013-5460-2.
19. Uthoff S, Stoveken T, Weber N, Vosmann K, Klein E, Kalscheuer R, Steinbuchel A. 2005. Thio wax ester biosynthesis utilizing the unspecific bifunctional wax ester synthase/acyl coenzyme A:diacylglycerol acyltransferase of Acinetobacter sp. strain ADP1. Appl Environ Microbiol 71:790–796. https://doi.org/10.1128/AEM.71.2.790-796.2005.
20. Rottig A, Zurek PJ, Steinbuchel A. 2015. Assessment of bacterial acyltransferases for an efficient lipid production in metabolically engineered strains of E. coli. Metab Eng 32:195–206. https://doi.org/10.1016/j.ymben.2015.09.016.
21. Xu L, Wang L, Zhou XR, Chen WC, Singh S, Hu Z, Huang FH, Wan X. 2018. Stepwise metabolic engineering of Escherichia coli to produce triacylglycerol rich in medium-chain fatty acids. Biotechnol Biofuels 11:177. https://doi.org/10.1186/s13068-018-1177-x.
22. Liang MH, Jiang JG. 2013. Advancing oleaginous microorganisms to produce lipid via metabolic engineering technology. Prog Lipid Res 52:395–408. https://doi.org/10.1016/j.plipres.2013.05.002.
23. Marella ER, Holkenbrink C, Siewers V, Borodina I. 2018. Engineering microbial fatty acid metabolism for biofuels and biochemicals. Curr Opin Biotechnol 50:39–46. https://doi.org/10.1016/j.copbio.2017.10.002.
24. Hernandez MA, Comba S, Arabolaza A, Gramajo H, Alvarez HM. 2015. Overexpression of a phosphatidic acid phosphatase type 2 leads to an increase in triacylglycerol production in oleaginous Rhodococcus strains. Appl Microbiol Biotechnol 99:2191–2207. https://doi.org/10.1007/s00253-014-6002-2.
25. Rowlett VW, Mallampalli V, Karlstaedt A, Dowhan W, Taegtmeyer H, Margolin W, Vitrac H. 2017. Impact of membrane phospholipid alterations in Escherichia coli on cellular function and bacterial stress adaptation. J Bacteriol 199. https://doi.org/10.1128/JB.00849-16.
26. Bontemps-Gallo S, Cogez V, Robbe-Masselot C, Quintard K, Dondeyne J, Madec E, Lacroix JM. 2013. Biosynthesis of osmoregulated periplasmic glucans in Escherichia coli: the phosphoethanolamine transferase is encoded by opgE. Biomed Res Int 2013:371429. https://doi.org/10.1155/2013/371429.
27. Lin F, Chen Y, Levine R, Lee K, Yuan Y, Lin XN. 2013. Improving fatty acid availability for bio-hydrocarbon production in Escherichia coli by metabolic engineering. PLoS One 8:e78595. https://doi.org/10.1371/journal.pone.0078595.
28. Shen X, Wang J, Wang J, Chen Z, Yuan Q, Yan Y. 2017. High-level de novo biosynthesis of arbutin in engineered Escherichia coli. Metab Eng 42: 52–58. https://doi.org/10.1016/j.ymben.2017.06.001.
29. Jackson BJ, Bohin JP, Kennedy EP. 1984. Biosynthesis of membrane-derived oligosaccharides: characterization of mdoB mutants defective in phosphoglycerol transferase I activity. J Bacteriol 160:976–981. https://doi.org/10.1128/JB.160.3.976-981.1984.
30. Fiedler W, Rotering H. 1985. Characterization of an Escherichia coli mdoB mutant strain unable to transfer sn-1-phosphoglycerol to membrane-derived oligosaccharides. J Biol Chem 260:4799–4806.
31. Banas W, Carlsson AS, Banas A. 2014. Effect of overexpression of PDAT gene on Arabidopsis growth rate and seed oil content. J Agric Sci 6. https://doi.org/10.5539/jas.v6n5p65.
32. Lázaro B, Villa JA, Santín O, Cabezas M, Milagre CDF, de la Cruz F, Moncalián G. 2017. Heterologous expression of a thermophilic diacylglycerol acyltransferase triggers triglyceride accumulation in Escherichia coli. PLoS One 12: e0176520. https://doi.org/10.1371/journal.pone.0176520.
33. Wu J, Du G, Chen J, Zhou J. 2015. Enhancing flavonoid production by systematically tuning the central metabolic pathways based on a CRISPR interference system in Escherichia coli. Sci Rep 5:13477. https://doi.org/10.1038/srep13477.
34. Marmon S, Sturtevant D, Herrfurth C, Chapman K, Stymne S, Feussner I. 2017. Two acyltransferases contribute differently to linolenic acid levels in seed oil. Plant Physiol 173:2081–2095. https://doi.org/10.1104/pp.16.01865.
35. Banaś W, Sanchez Garcia A, Banaś A, Stymne S. 2013. Activities of acyl-CoA:diacylglycerol acyltransferase (DGAT) and phospholipid: diacylglycerol acyltransferase (PDAT) in microsomal preparations of developing sunflower and safflower seeds. Planta 237:1627–1636. https://doi.org/10.1007/s00425-013-1870-8.
36. Studier FW. 2005. Protein production by auto-induction in high density shaking cultures. Protein Expr Purif 41:207–234. https://doi.org/10.1016/j.pep.2005.01.016.
37. Jiang Y, Chen B, Duan C, Sun B, Yang J, Yang S. 2015. Multigene editing in the Escherichia coli genome via the CRISPR-Cas9 system. Appl Environ Microbiol 81:2506–2514. https://doi.org/10.1128/AEM.04023-14.
38. Sharan SK, Thomason LC, Kuznetsov SG, Court DL. 2009. Recombineering: a homologous recombination-based method of genetic engineering. Nat Protoc 4:206–223. https://doi.org/10.1038/nprot.2008.227.
39. Katoh K, Misawa K, Kuma K, Miyata T. 2002. MAFFT: a novel method for rapid multiple sequence alignment based on fast Fourier transform. Nucleic Acids Res 30:3059–3066. https://doi.org/10.1093/nar/gkf436.
40. Siedler S, Schendzielorz G, Binder S, Eggeling L, Bringer S, Bott M. 2014. SoxR as a single-cell biosensor for NADPH-consuming enzymes in Escherichia coli. ACS Synth Biol 3:41–47. https://doi.org/10.1021/sb400110j.
41. Letunic I, Bork P. 2016. Interactive tree of life (iTOL) v3: an online tool for the display and annotation of phylogenetic and other trees. Nucleic Acids Res 44:W242–5. https://doi.org/10.1093/nar/gkw290.
42. Chen C, Xia R, Chen H, He Y. 2018. TBtools, a toolkit for biologists integrating various HTS-data handling tools with a user-friendly interface. bioRxiv https://doi.org/10.1101/289660.
43. Kelley LA, Mezulis S, Yates CM, Wass MN, Sternberg MJ. 2015. The Phyre2 web portal for protein modeling, prediction and analysis. Nat Protoc 10:845–858. https://doi.org/10.1038/nprot.2015.053.
44. Trott O, Olson AJ. 2010. AutoDock Vina: improving the speed and accuracy of docking with a new scoring function, efficient optimization, and multithreading. J Comput Chem 31:455–461. https://doi.org/10.1002/jcc.21334.
45. Morris GM, Huey R, Lindstrom W, Sanner MF, Belew RK, Goodsell DS, Olson AJ. 2009. AutoDock4 and AutoDockTools4: automated docking with selective receptor flexibility. J Comput Chem 30:2785–2791. https://doi.org/10.1002/jcc.21256.
46. Xiao K, Yue XH, Chen WC, Zhou XR, Wang L, Xu L, Huang FH, Wan X. 2018. Metabolic engineering for enhanced medium chain omega hydroxy fatty acid production in Escherichia coli. Front Microbiol 9:139. https://doi.org/10.3389/fmicb.2018.00139.